POLITECNICO
MILANO 1863

DIPARTIMENTO DI MECCANICA

mecc

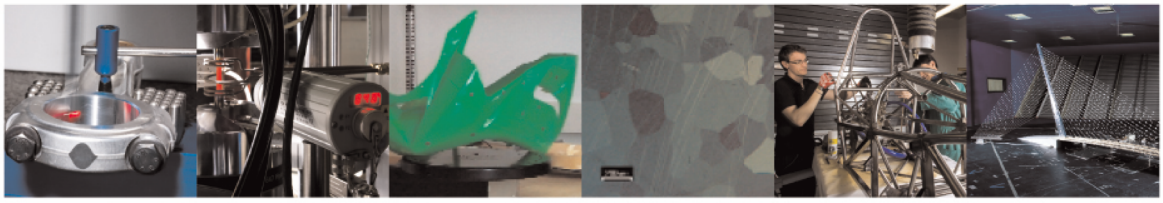

Energy method to compute the maximum amplitudes of oscillation of bundle conductors due to ice galloping

Giorgio Diana, Alessandra Manenti, and Stefano Melzi

This is a post-peer-review, pre-copyedit version of an article published in *IEEE Transactions on Power Delivery*. The final authenticated version is available online at: http://dx.doi.org/10.1109/TPWRD.2020.3027157

DIPARTIMENTO DI MECCANICA ■ POLITECNICO DI MILANO
via G. La Masa, 1 ■ 20156 Milano ■ EMAIL (PEC): pecmecc@cert.polimi.it
http://www.mecc.polimi.it
Rev. 0

Energy method to compute the maximum amplitudes of oscillation of bundle conductors due to ice galloping

Giorgio Diana, *Member, IEEE*, Alessandra Manenti, and Stefano Melzi, *Member, IEEE*

***Abstract*-- The paper presents a modal model to describe the interaction between a 4-conductor bundle and wind. A finite-element model of the bundle is used to perform a linear analysis, to extract mode shapes and natural frequencies of the system. The motion of the expanded bundle is then described through mode coordinates representing the first horizontal, vertical and torsional modes. Wind tunnel tests were performed adding templates over the cables to mimic the presence of ice over the same conductor bundle; tests allowed to characterize the aerodynamic coefficients of the entire bundle and provided data for the model validation. The model was then applied to a case study to predict the maximum oscillations produced by ice galloping. Time-domain simulations were used for the purpose, together with an alternative approach named energy method; this last directly estimates the amplitude of limit cycles avoiding the integration of the equations of motion and can be much more useful from the engineering point of view.**

***Index Terms*—bundle conductors, galloping, oscillation amplitudes, modal model, energy method, wind tunnel**

I. Introduction

Ice galloping on High Voltage (HV) Over Head Transmission Lines (OHTL) is a very well-known phenomenon, causing a lot of problems with flash-overs and conductor and towers failure. A lot of papers have been published on the subject [1][2][3][4]: a good reference is the EPRI Transmission Lines Reference Book (Orange Book) [5] in which chapter 4 – written by P.Van Dyke, JL Lilien and D.Havard – is dedicated to the description of the phenomenon and reports the state-of-the–art of the knowledge on it.

Galloping occurs both in single and bundle conductors. On single conductors it can be mainly described as a one-degree-of-freedom instability – as for the first time reported by Den Hartog in 1932 [6] due to the negative value of the slope of the lift aerodynamic coefficient. On bundle conductors, together with the one-degree-of-freedom instability, a two-degrees of-freedom instability may occur. This paper is mainly focused on bundle conductors, that have become more and more important in the HV Transmission Lines. In any case, the approach presented in the paper can be also applied to the case of the single conductor.

Many different approaches can be found in literature to simulate ice-galloping on bundle conductors, the most of them using Finite Element Modelling (FEM) to reproduce the structural part of the system (single of multi-span sections of the transmission Line) and relying on the Quasi Steady Theory (QST) to reproduce the fluid-elastic forces [7][8].The QST uses the static lift, drag and moment coefficients of the bundle with ice formation on the conductors measured in wind tunnel as a function of the angle of attack of the wind. This approach can be very useful to define what kind of device can be used to control the different types of instabilities that may occur: one-degree-of-freedom or Den Hartog instability and two-degrees of freedom or flutter type instability. With this approach, it is possible to verify that increasing the damping of the system – for instance by using a Tuned Mass Damper (TMD) – the problem can be controlled. Unfortunately it is not easy to design a damper for frequencies as in the range 0.2-0.3 Hz, typical of ice-galloping oscillations. The problem is worsened by the presence of ice-formations which may also affect the damper performance.

The detuning pendulum has been widely used to try to control ice-galloping in bundles: in this case the pendulum increases the torsional frequency of the bundle and increases the critical wind speed associated with instability onset. The best instrument to design the type, number and position of these devices is the FEM approach based on the QST [4] [9]. In any case the big difficulty is to know what type of ice formations have to be considered in the different cases and consequently define the lift, drag and moment coefficients for all the different ice shapes as a function of the wind angle of attack.

Another problem is that numerical codes based on the FEM approach and the QST work in the time domain and, as a consequence, a lot of time is needed for the simulations to reach steady state amplitudes of oscillation. So these programs are not suitable to be used at an engineering level to assess the ice-galloping severity and to identify the correct counter-measures to control the phenomenon.

G. Diana is with the Department of Mechanics, Politecnico di Milano, Via La Masa 1, 20153 Milano, Italy (e-mail: giorgio.diana@polimi.it).
A. Manenti is with the Department of Mechanics, Politecnico di Milano, Via La Masa 1, 20153 Milano, Italy (e-mail: alessandra.manenti@polimi.it).
S. Melzi is with the Department of Mechanics, Politecnico di Milano, Via La Masa 1, 20153 Milano, Italy (e-mail: stefano.melzi@polimi.it).

Scope of this paper is to present a numerical approach also based on FEM of the bundle conductors and using the QST for the fluid-dynamic forces, as those previously described, but aiming at directly find the amplitude of a limit cycle instead of identifying it from the time-domain simulations. This approach, named energy method (EM), allows to estimate the maximum amplitudes of oscillation due to ice galloping as a function of the wind speed. The validity of the presented method is verified through comparison with the results of the approach working in the time domain. Moreover the validity of the used in our approach is confirmed by two factors:

1. the reduced velocity $V_r = \frac{U}{cf}$ is much greater than 15 where the QST is considered valid. In the definition of Vr, U is the wind speed, c a reference dimension of the body (in our case the bundle separation in the order of 0.5 m) and f is the frequency of the bundle motion generally lower than .5 Hz. The reduced velocity for a wind speed greater than 6 m/s, below which the ice galloping do not occur, is always greater than 15.
2. As reported in paragraph III, the QST has been also validated through wind tunnel test on a sectional model of the bundle. Free to vibrate in horizontal, vertical and torsional direction.

The proposed method is based on an energy balance: amplitudes of vibration are computed equaling the energy introduced by wind forces and the energy dissipated by conductors in one limit cycle. The energy method can be profitably used to design and verify the effect of controlling devices like detuning pendulums and interphase spacers.

It has to noted that – as reported in the EPRI Orange Book - some attempts to compute in an easy way the maximum amplitudes of ice-galloping as a function of the wind speed have been already made [7][8]. All of these methods are mainly based on very simple formulations that cannot take into account all the complexity of the problem, especially when the type of instability is due to the combination of torsional and vertical modes of vibration, as mainly occurs in bundle conductors.

The paper is organized in the following sections: 1) description of the numerical model, 2) validation of the numerical model, 3) application of numerical model to a case study, 4) description and application of the energy method.

II. Numerical Model

A. FEM model of the bundle

A detailed description of the numerical model of the conductor bundle is reported in [11]; the main details are hereafter presented. The numerical model of the bundle is based on a finite element scheme: stranded-beam elements (6 degrees of freedom per node) are used to reproduce the flexural, torsional and tensile response of each conductor. I-type or V-type insulators are introduced at the extremities of the bundle span; rigid beams connect the conductors ends to a node located at the center of the bundle which is then linked to the insulator. A lumped-parameter model is adopted to describe the effect of spacers that may be introduced in generic positions along the span. The inertia of a spacer is concentrated in a central body and in clamps elements; these lasts are connected to the central body through springs and dampers to reproduce the behavior of the spacer dampers generally used in bundle systems. The motion of the spacer is assumed to take place in a plane normal to the longitudinal direction of the bundle; its mass, damping and stiffness matrices are condensed and added to the corresponding matrices of the bundle structure.

B. Modal analysis of the bundle

The finite element scheme generated as described in the previous section is used to determine the span deformation due to its own weight. An iterative algorithm is adopted to compute the equilibrium configuration where the tensile preload of finite elements changes along the span due to the effect of gravity. Tensile preload modifies the stiffness of beam elements and therefore the overall stiffness matrix.

Once the static configuration is defined, the natural frequencies and the vibration modes of the bundle are estimated numerically, focusing the attention on the typical frequency range of galloping, i.e. below 1 Hz. The process leads to determine the mode shapes in terms of displacements of the nodes of each element of the scheme.

The idea proposed in the paper is to describe the motion of the entire bundle using a modal superposition approach but referring the mode shapes to an equivalent super-conductor. When dealing with instability associated with ice formation over the cables of a bundle, relative displacements among them are in fact negligible; this means that, as first approximation, each section of the bundle along the span behaves like the cables were part of a rigid body. Following this assumption, the positions of the conductors of the *j-th* section of the bundle referred to the *k-th* mode shape can thus be expressed as a combination of the translation of the center of the section along the horizontal and vertical directions ($Y_{j,k}$, $Z_{j,k}$) and a rotation around the section center ($\theta_{j,k}$). Minimizing the differences between the displacements of the cables of the *k-th* mode shape and those obtained with the rigid body model, leads to identification of $Y_{j,k}$, $Z_{j,k}$ and $\theta_{j,k}$.

The process is repeated for all the sections defined over the bundle span. The *k-th* mode shape of the super-conductor can be represented through the vector $\mathbf{\Phi_k}$ defined as follows:

$$\mathbf{\Phi_k} = \left[\mathbf{\Phi_{ky}} \quad \mathbf{\Phi_{kz}} \quad \mathbf{\Phi_{k\theta}}\right]^T \tag{1}$$

where $\mathbf{\Phi_{ky}}$ collects the displacements along horizontal direction, $\mathbf{\Phi_{kz}}$ the displacements along vertical direction and $\mathbf{\Phi_{k\theta}}$, the rotations of the sections. This easily leads to the definition of the matrix of mode shapes:

$$\left[\mathbf{\Phi}\right] = \left[\mathbf{\Phi}_1 \quad \mathbf{\Phi}_2 \quad \ldots \quad \mathbf{\Phi}_n\right] \tag{2}$$

The motion of the bundle is assumed to be conveniently described through *n* mode coordinates corresponding to the first *n* modes of the super-conductor.

C. Wind-bundle interaction

The aerodynamic forces are modeled considering the quasi-static theory [10] and generating space-time wind profile (horizontal and vertical components) starting from a Power Spectral Density function based of the wind characteristics in terms of: mean velocity U, turbulence intensity $I=\sigma_u/U$ and space correlation introduced through the integral scales L_{uz} and L_{wz} [11]. Being v_j the relative speed between wind and super-conductor in the *j-th* section of the finite element scheme, aerodynamic drag ($F_{d,j}$), lift ($F_{l,j}$) and moment ($M_{x,j}$) are assumed to be expressed as reported in (3), where a four-conductor bundle was considered. In equation (3), ρ represents the air density, D the diameter of the single cable of the bundle and L_j the length *j-th* segment of cable; c is the bundle chord, defined by the span of cables along the horizontal direction.

$$\begin{cases} F_{d,j} = \frac{1}{2}\rho 4DL_j C_d(\alpha_j) v_j^2 \\ F_{j,j} = \frac{1}{2}\rho 4DL_j C_l(\alpha_j) v_j^2 \\ M_{x,j} = \frac{1}{2}\rho 4DL_j C_m(\alpha_j) c v_j^2 \end{cases} \quad (3)$$

The aerodynamic coefficients C_d, C_l and C_m are function of the angle of attack α_j and are referred to the entire bundle. Tests were carried out in the wind tunnel to measure these coefficients for different bundle arrangements and different cross sections of the cables. For instance, Fig. 1 reports the aerodynamic coefficients measured on a bundle made up of four cables arranged on the vertexes of a 0.5 m-side square.

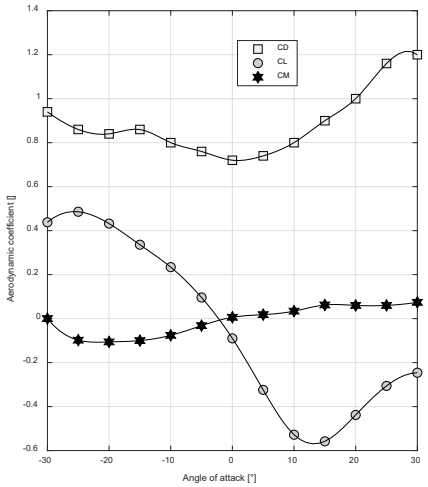

Fig. 1 Aerodynamic coefficients for a 0.5m-side square bundle

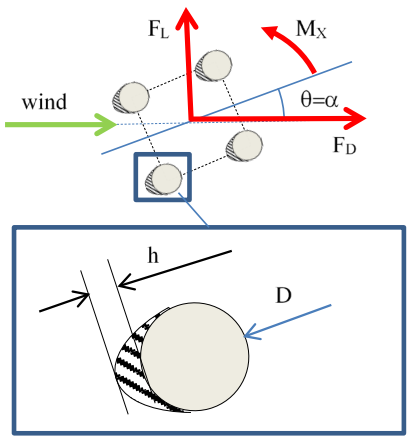

Fig. 2 conventions and cross section of a cable: D=31 mm, h=10 mm.

The conventions used for the angle of attack and forces are shown in Fig. 2, together with the cross section of the conductor. Tests for measuring aerodynamic coefficients were carried out applying different rigid rotations θ to the entire bundle while it was hit by a horizontal wind with constant speed. In the test configuration the angle of attack α coincides with the rigid rotation of the bundle θ. The lower part of Fig. 2 depicts the cross section of a cable putting into evidence the templates added to reproduce the presence of ice on the leading edges.

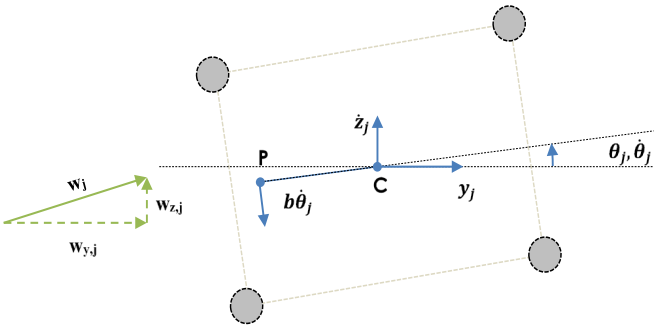

Fig. 3 interaction between wind and super-conductor

Referring to Fig. 3 the speed of the turbulent wind acting on the *j-th* section of the super-conductor is defined by the horizontal component $w_{y,j}$ and a vertical component $w_{z,j}$. The relative speed with respect to the super-conductor is computed considering the speed of the point P whose position is identified on the basis of experimental data collected in wind tunnel tests. Assuming a symmetrical distribution of the cables of the bundle along the vertical direction, position of P can be identified by the distance b, as shown in Fig. 3. The speed of P can be then obtained summing up the motion of the center of the super-conductor (point C) and its relative motion with respect to this point, that is:

$$\begin{aligned} v_{Py,j} &= \dot{y}_j + b\dot{\theta}\sin\theta_j \\ v_{Pz,j} &= \dot{z}_j - b\dot{\theta}\cos\theta_j \end{aligned} \quad (4)$$

The terms of (4) can be derived from vector the mode coordinates **q**.

$$\dot{y}_j = \mathbf{\Phi_{y,j}}\dot{\mathbf{q}}; \quad \dot{z}_j = \mathbf{\Phi_{z,j}}\dot{\mathbf{q}}; \quad \dot{\theta}_j = \mathbf{\Phi_{\theta,j}}\dot{\mathbf{q}}; \tag{5}$$

where $\mathbf{\Phi_{y,j}}$ is the vector of mode shapes along horizontal direction for the *j-th* section of the super-conductor. $\mathbf{\Phi_{z,j}}$ and $\mathbf{\Phi_{\theta,j}}$ have an analogous meaning but are referred to vertical displacement and rotation of *j-th* section. The relative speed between wind and super-conductor can thus be obtained.

$$\begin{cases} v_{y,j} = w_{y,j} - \dot{y}_j - b\dot{\theta}\sin\theta_j \\ v_{z,j} = w_{z,j} - \dot{z}_j + b\dot{\theta}\cos\theta_j \end{cases} \tag{6}$$

This allows determining the modulus of relative v_j speed the inclination of the wind ψ_J with respect to the horizontal direction and the angle of attack α_j.

$$v_j = \sqrt{\left(v_{y,j}^2 + v_{z,j}^2\right)}; \quad \psi_j = \arctan\frac{v_{z,j}}{v_{y,j}}; \alpha_j = \psi_j - \theta_j \tag{7}$$

It is now possible to compute the aerodynamic forces and moments acting on the *j-th* section of the super-conductor

$$\begin{cases} F_{y,j} = \frac{1}{2}\rho 4DL_j\left[C_d(\alpha_j)\cos\psi_j - C_l(\alpha_j)\sin\psi_j\right]v_j^2 \\ F_{z,j} = \frac{1}{2}\rho 4DL_j\left[C_d(\alpha_j)\sin\psi_j + C_l(\alpha_j)\cos\psi_j\right]v_j^2 \\ M_{x,j} = -\frac{1}{2}\rho 4DL_j C_m(\alpha_j)cv_j^2 \end{cases} \tag{8}$$

The aerodynamic forces and moments can be conveniently collected in a unique vector $\mathbf{F_a}(\mathbf{q},\dot{\mathbf{q}},t)$; the virtual work of aerodynamic forces can thus be expressed as:

$$\delta L = \mathbf{F_a}(\mathbf{q},\dot{\mathbf{q}},t)[\mathbf{\Phi}]\delta\mathbf{q} = \mathbf{Q_a}(\mathbf{q},\dot{\mathbf{q}},t)^T\,\delta\mathbf{q} \tag{9}$$

where the explicit dependence on time is due to the time histories of wind speeds acting on different sections of the bundle. Equation of motion of the super-conductor are eventually assembled as follows:

$$[\mathbf{M}]\ddot{\mathbf{q}} + [\mathbf{R}]\dot{\mathbf{q}} + [\mathbf{K}]\mathbf{q} = \mathbf{Q_a}(\mathbf{q},\dot{\mathbf{q}},t) \tag{10}$$

where **[M], [R]** and **[K]** are diagonal matrices containing mode mass, damping and stiffness of each eigenmode; the damping matrix is obtained as a linear combination of mass and stiffness matrices.

III. Validation of the Numerical Model

The model described in the previous paragraphs was implemented in a numerical code and tested against experimental data collected in a series of wind tunnel tests. During the same test sessions, the aerodynamic coefficients reported in Fig. 1 were measured.

The main target of the experimental tests was the characterization of the static aerodynamic coefficients of a four-conductor bundle investigating the effect of ice formation. The base experimental set-up was made up of 4 rigid conductors arranged on the vertexes of a 0.5 m-side square (Fig. 4). Relative displacements among conductors were negligible. Each conductor was 0.95 meter long and had a diameter of 31 mm. The presence of ice formation was artificially produced by adding templates of suitable shapes, like the one shown in Fig. 2.

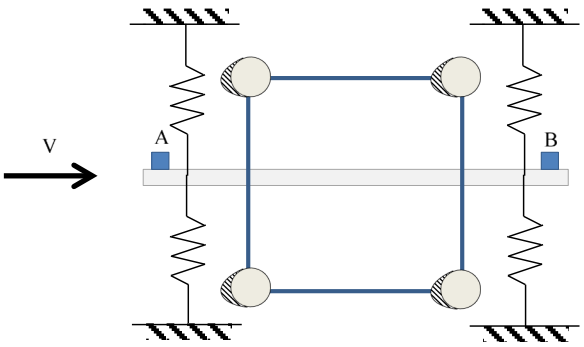

Fig. 4 set-up for the characterization of flutter instability.

Besides the tests performed for the identification of static aerodynamic coefficients referred to a section of the bundle, additional tests were carried out to investigate the onset of flutter instability associated with the coupling of vertical and torsional motion of the entire bundle. For the purpose, the set-up shown in Fig. 4 was used. The bundle was suspended with elastic elements whose parameters were tuned to obtain reasonable values eigenfrequencies, as if the section tested in wind tunnel was part of a longer suspended bundle. Two accelerometers (A and B in Fig. 4) were added to characterize the response of the bundle in terms of vertical and torsional dynamics. The main features of the experimental set-up are collected in TABLE 1.

TABLE 1
Main features of the experimental set-up

Conductor diameter	0.031 m
Conductor length	0.95 m
Conductor spacing	0.5 m
Horizontal frequency	0.5 Hz
Vertical frequency	0.88 Hz
Torsional frequency	0.97 Hz
Damping factor	1‰
Distance A-B	0.93 m

Experimental data showed that flutter instability triggers for wind speeds above 17 m/s; an example of the build-up of the oscillation (rotation around the longitudinal axis) referred to a wind speed of 18.5 m/s is reported in Fig. 5.

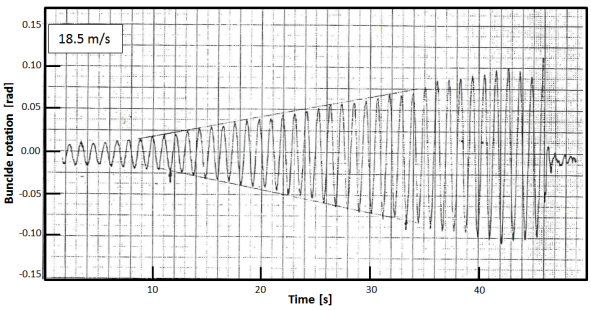

Fig. 5 oscillation build-up of the bundle with a wind speed of 18.5 m/s.

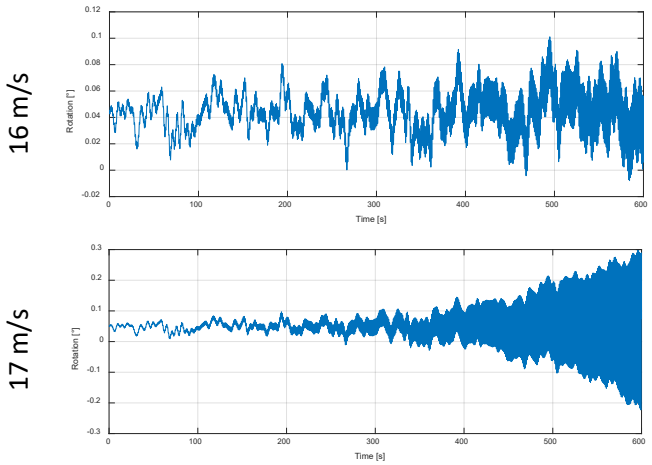

Fig. 6 time histories of bundle oscillation for different wind mean speeds.

The numerical model was used to reproduce the same conditions of experimental tests. The motion of the bundle was described combining three rigid modes (horizontal displacement, vertical displacement and rotation around the longitudinal axis) using the frequencies and damping factors reported in Table 1. Several simulations were performed for mean wind speeds from 16 to 20 m/s; a turbulence index of 1% was assumed. The output of numerical results is consistent with the experiments: instability appears for speeds above 17 m/s. Fig. 6 reports the time histories of bundle oscillation for wind speeds of 16 m/s and 17 m/s. The upper graph (16 m/s) does not reveal signs of instability, while increasing wind speed by just 1 m/s leads to a significantly different response characterized by a progressive increase of bundle oscillation.

Results of comparisons are collected in Table 2 and show that the model is able to reproduce the experimental behaviour with satisfying precision. The frequency of the instable motion is slightly overestimated by the model, showing a decreasing trend with wind speed. Damping factor are comparable: the numerical model displays an increase of the absolute value with speed which is consistent with experimental behaviour. As far as the dynamics of the two measuring points is concerned, the numerical model slightly overestimates the ratio between the amplitudes of acceleration of point B and A. The relative phase, reported in the last columns, is instead very similar. Altogether the agreement between experimental and numerical data appears satisfying; in particular the numerical model is able to catch the instability threshold in terms of wind speed. Both experimental and numerical results reveal a flutter type instability. The torsional frequency decreases due to the aerodynamic force field and becomes close to the vertical one, giving rise to flutter instability.

TABLE 2
Comparison between experimental and numerical results.

		17.7 m/s	18.5 m/s	19.8 m/s
Frequency	Exp.	0.92 Hz	0.92 Hz	0.90 Hz
	Num.	0.95 Hz	0.95 Hz	0.94 Hz
Damping factor	Exp.	-3‰	-8‰	-25‰
	Num.	-6‰	-10‰	-16‰
Amplitude B/A	Exp.	2.2	2.4	2.6
	Num.	3.8	3.6	2.9
Phase B-A	Exp.	-30°	-35°	-35°
	Num.	-29°	-31°	-28°

IV. A CASE STUDY

The numerical model was used to analyze the dynamics of a 4-conductor bundle; in particular, the goal is to identify maximum oscillation amplitudes associated with ice-galloping comparing two numerical methods: the first one based on solving motion equations in time domain waiting for the system to reach a steady state oscillation, the second one based on direct search for the same condition on the basis of energetic balance. The main characteristics of the bundle are reported in Table 3.

The section of the bundle is identical to that of the experimental set-up of wind tunnel tests. In this case a span of 400 m is assumed and the bundle is modeled with a series stranded-beam elements allowing to reproduce the cable flexibility. 7 spacers are evenly distributed along the span (1 spacer each 50 m). Quasi-static theory previously described is adopted to describe the aerodynamic forces and aerodynamic coefficients reported in Fig. 1 are assumed; this means the response induced by ice-formations over the cables may couple vertical and torsional dynamics of the cables.

TABLE 3
Main characteristics of the bundle analyzed in the case study..

Cable diameter	30 mm
Mass per unit length	1.6 [kg/m]
Pre-tensioning load	28070 N
Number of cables	4
Cable arrangement	Square; side 0.5 m
Span length	400
Number of spacers	7 (one each 50 m)
Suspension	I-type (5m)

As first step, the finite element model was used to determine the eigenfrequencies and eigenmodes of the bundle, computed around the static equilibrium position. Table 4 collects the frequencies and the description of the associated modes resulting from the computation. These modes range from 0.12 to 0.5 Hz and include 2nd and 3rd vertical and torsional modes.

TABLE 4
Frequencies and description of the first 8 modes of the bundle.

Mode	Frequency	Description
1	0.125 Hz	1st horizontal

2	0.241 Hz	2nd horizontal
3	0.283 Hz	2nd vertical
4	0.337 Hz	2nd torsional
5	0.368 Hz	3rd horizontal
6	0.394 Hz	3rd vertical
7	0.397 Hz	3rd torsional
8	0.500 Hz	4th horizontal

The modes reported in Table 4 were used to describe the motion of the bundle through the mode approach presented before. For the purpose, the damping matrix **[R]** was obtained as a linear combination of mass and stiffness matrix, that is:

$$[\mathbf{R}] = \alpha[\mathbf{M}] + \beta[\mathbf{K}] \tag{11}$$

Values for α and β were chosen to have damping factors between 0.1÷0.3‰ over the selected modes.

A. Linear analysis

A preliminary linear analysis can be performed aiming at computing the eigenvalues of the system for different wind speeds. Despite the approximations introduced by linearization, this last allows to get an overall picture of the onsets of instabilities with increasing wind speed and of the frequencies associated with unstable modes. After setting a value for the mean wind speed, a static solution $\mathbf{q_s}$ for equation (10) is determined, so that:

$$[\mathbf{K}]\mathbf{q_s} = \mathbf{Q_a}(\mathbf{q_s}, \mathbf{0}) \tag{12}$$

Equation (12) is solved numerically; equation (10) is then linearized around the static solution:

$$[\mathbf{M}]\ddot{\bar{\mathbf{q}}} + [\mathbf{R}]\dot{\bar{\mathbf{q}}} + [\mathbf{K}]\bar{\mathbf{q}} + [\mathbf{K}]\mathbf{q_s} \approx \mathbf{Q_a}(\mathbf{q_s}, \mathbf{0}) - [\mathbf{R_a}]\dot{\bar{\mathbf{q}}} - [\mathbf{K_a}]\bar{\mathbf{q}} \tag{13}$$

where $\bar{\mathbf{q}}$ is defined as $\mathbf{q} - \mathbf{q_s}$ and

$$[\mathbf{K_a}] = -\begin{bmatrix} \frac{\partial Q_{a1}}{\partial q_1} & \cdots & \frac{\partial Q_{a1}}{\partial q_n} \\ \cdots & \cdots & \cdots \\ \frac{\partial Q_{an}}{\partial q_1} & \cdots & \frac{\partial Q_{an}}{\partial q_n} \end{bmatrix}; \quad [\mathbf{R_a}] = -\begin{bmatrix} \frac{\partial Q_{a1}}{\partial \dot{q}_1} & \cdots & \frac{\partial Q_{a1}}{\partial \dot{q}_n} \\ \cdots & \cdots & \cdots \\ \frac{\partial Q_{an}}{\partial \dot{q}_1} & \cdots & \frac{\partial Q_{an}}{\partial \dot{q}_n} \end{bmatrix} \tag{14}$$

Elements of matrices $[\mathbf{K_a}]$ and $[\mathbf{R_a}]$ are estimated numerically considering ratios between variations of $\mathbf{Q_{ak}}$ associated with small variations of the mode coordinates and speeds. The linearized motion equation around static equilibrium thus becomes:

$$[\mathbf{M}]\ddot{\bar{\mathbf{q}}} + [[\mathbf{R}] + [\mathbf{R_a}]]\dot{\bar{\mathbf{q}}} + [[\mathbf{K}] + [\mathbf{K_a}]]\bar{\mathbf{q}} = \mathbf{0} \tag{15}$$

A linear analysis of the free response of the system is then carried out to compute the eigenvalues of the damped system. Eigenvalues with positive real part are identified so that the onset of unstable modes for different wind speeds can be revealed.

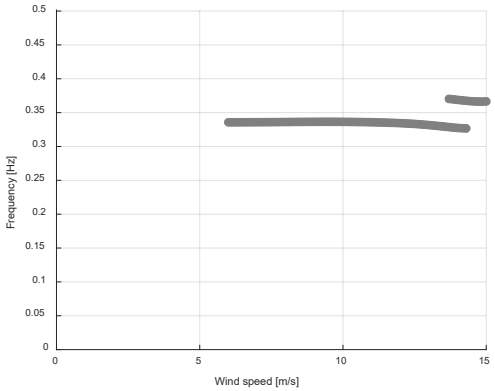

Fig. 7: frequency of unstable modes as function of wind speed.

Fig. 7 refers to the case study and shows the frequency of the eigenvalues with positive real part for wind speeds up to 15 m/s (~55 km/h); two eigenvalues with positive real part are reveled in this speed range. The first instability appears for wind speeds above 6 m/s with a frequency of 0.336 Hz. The frequency of the instability gradually decreases down to 0.326 Hz for a wind speed of 14.3 m/s. The frequency value and its decreasing trend suggest that instability is related to a combination of the 2nd torsional and 2nd vertical modes of Table 4. This instability is no longer present for wind speeds above 14.3 m/s. The second instability appears at 13.7 m/s with an initial frequency of 0.370 Hz that decreases to 0.366 Hz at 15m/s. Looking again at Table 4, the instability is reasonably due to a combination of modes 6 and 7, i.e. the 3rd vertical mode and the 3rd torsional mode.

A. Time-domain simulations

Several simulations were carried out generating time histories of wind considering different mean wind speeds and assuming a turbulence index of 1%, practically corresponding to no turbulence. The main purpose of simulations was to put into evidence the role of mean wind speed in affecting the onset of instabilities related with ice galloping and estimating oscillation amplitudes associated with the phenomenon.

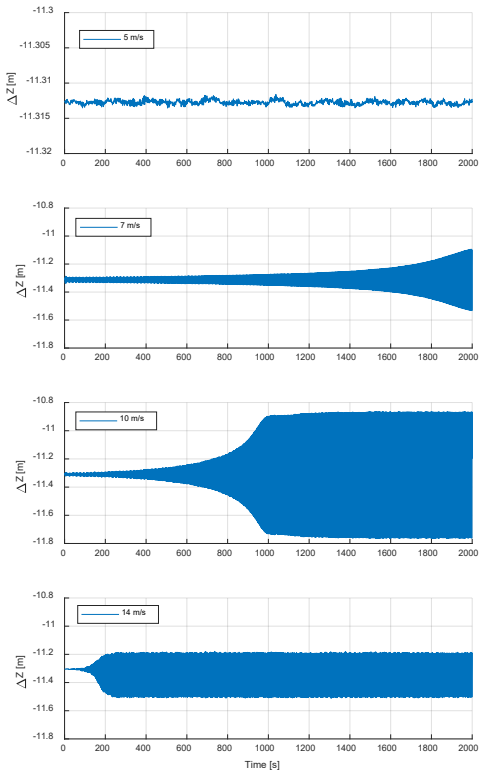

Fig. 8 bundle with nominal parameters. Vertical displacement and rotation of the section at 100 m for different wind speeds.

Fig. 8 shows the response of a section of the bundle in terms of vertical displacement as function of time. Results refer to a section at ¼ of the span length, a location where the 2nd vertical mode presents an antinode. The chart on the top is obtained with a wind speed of 5 m/s and shows small oscillations around the equilibrium position in the order of ±1cm. When the wind speed rises to 7 m/s, the response changes significantly: oscillations gradually expand reveling an unstable behavior. A limit cycle is eventually reached after 3000 s (not reported in the graph), with regime amplitudes of nearly ±25cm. Increasing the wind speed up to 10 m/s leads to a faster transient toward a limit cycle with larger oscillations (±45cm). A further increase of wind speed up to 14 m/s reveal an even faster transient but towards smaller oscillations, again around ±15cm.

The analysis of the spectra of the regime oscillation of the last three simulations (Fig. 9), provides a better insight on the response of the bundle. For a wind speed of 7 m/s, the spectrum presents a clear dominant harmonic component at 0.334 Hz with an amplitude of 0.22 m. For a wind speed of 10 m/s the spectrum looks similar with a dominant harmonic at 0.332 Hz and an amplitude of 0.43 m. The frequency of these peaks is close to the one of the 2nd torsional mode; the decreasing trend of frequency with wind speed suggests that the aerodynamic coefficients due to ice formations are able to decrease the torsion stiffness of the super-conductor. When the wind speed rises at 14 m/s, the spectrum shows a smaller peak at 0.376 Hz while no significant contribution is evidenced around 0.33 Hz. The higher frequency is close to the one of the 3rd torsional mode; therefore, the instability around 0.33 Hz disappeared and oscillations are now associated with the instability of modes 6-7 combined.

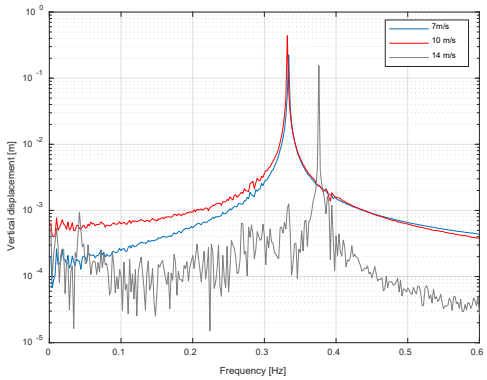

Fig. 9 FFT modulus of the section at 100 m for different wind speeds.

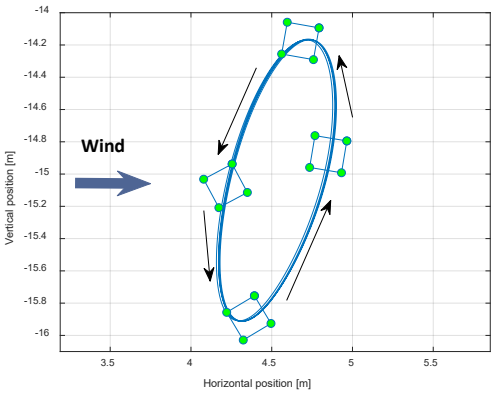

Fig. 10 limit cycle for the section at mid span; wind speed 15 m/s.

Altogether, the time domain simulations confirm the results of the preliminary linear analysis. An instability associated with a combination of 2nd vertical and 2nd torsional mode appears for wind speeds between 5 and 7 m/s. This instability vanishes for speed higher than 13 m/s. At 14 m/s, a second instability associated with a combination of 3rd vertical and 3rd torsional mode is triggered.

Time-domain simulations can conveniently be used to determine the maximum oscillation amplitudes of the cable for different mean wind speeds. For speeds below 13 m/s maximum oscillations are associated with 2nd torsional-2nd vertical modes and are in the order of 0.6 m. For higher speeds, instability is associated with 3rd torsional-3rd vertical modes and maximum oscillations are in the order of 0.9 m.

Fig. 10 shows the limit cycle of the section at mid span for a wind mean speed of 15 m/s; the vertexes of the squares represent the positions of the four conductors (though their relative distance was reduced to make the picture more clear). It can be seen how the rotation of the super-conductor combines with the vertical motion allowing lift force to introduce energy during the descending and ascending phases

V. Energy Method

Though the modal approach allows reducing the number of degrees of freedom of the system, time-domain simulations still result demanding in terms of computational time; being the

structural damping of the bundle very low, a significant oscillation amplitude has to be reached to achieve an equilibrium between the energy introduced by the aerodynamic forces and the energy dissipated by damping forces. Moreover, when parametric analyses are performed, for example to investigate the effect of positions and parameters of detuning pendulums or interphase spacers on ice galloping, the number of simulations can easily increase. Time-domain simulations cannot be considered a practical tool to optimize the design of these devices. Due to this reason, an *energy method* was developed to obtain a faster estimation of the maximum oscillation amplitudes of the bundle as function of the wind speed. The method is described in the following.

As first step, starting from the linear analysis, the pairs of vertical and torsional modes that combine generating instability in the frequency range below 0.5 Hz are found. Let's identify these modes with $\mathbf{\Phi_{Vm}}$ and $\mathbf{\Phi_{Tm}}$, i.e.: the vectors of mode shapes for the vertical and torsional mode respectively. The subscript *m* refers to the *m-th* instability resulting from the linear analysis where the order is determined by the speed v_m that triggers the unstable mode. Considering the data of Table 4, the first instability (m=1) is associated with a combination of the 2nd vertical ($\mathbf{\Phi_{V1}}$) and 2nd torsional ($\mathbf{\Phi_{T1}}$) modes, while the second instability (m=2) is related with a combination of the 3rd vertical ($\mathbf{\Phi_{V2}}$) and 3rd torsional ($\mathbf{\Phi_{T2}}$) modes. The procedure can be obviously extended to other unstable modes if present. When the instability develops into a limit cycle, the motion of the bundle is assumed to be described with a combination of the mode shapes $\mathbf{\Phi_{Vm}}$ and $\mathbf{\Phi_{Tm}}$. This means that the motion of the generic *j-th* section of the bundle can be written as:

$$\mathbf{x_j}(t) \cong \mathbf{\Phi_{Vm,j}}\bar{q}_V(t) + \mathbf{\Phi_{Tm,j}}\bar{q}_T(t) \tag{16}$$

being $\mathbf{x_j}$ the vector collecting the horizontal displacement, the vertical displacement and the rotation of the *j-th* section of the bundle:

$$\mathbf{x}_j(t) = \left[y_j(t) \quad z_j(t) \quad \theta_j(t)\right]^T \tag{17}$$

In (16) $\bar{q}_V(t)$ and $\bar{q}_T(t)$ respectively represent the vertical and torsional mode coordinates corresponding to the mode shapes $\mathbf{\Phi_{Vm}}$ and $\mathbf{\Phi_{Tm}}$. For the two mode coordinates to describe a limit cycle, their expression is assumed to be:

$$\begin{cases} \bar{q}_V(t) = \alpha Q_{Vm0}\cos(\omega_m t) \\ \bar{q}_T(t) = \alpha Q_{Tm0}\cos(\omega_m t + \psi_m) \end{cases} \tag{18}$$

In (18) ω_m represents the angular frequency of the *m-th* unstable mode; Q_{Vm0} and a Q_{Tm0} are the amplitudes of the vertical and torsional mode coordinates resulting from the modal analysis for the same mode, i.e.: considering the 1st unstable mode, Q_{Vm0} would be the amplitude of the mode coordinate associated with the 2nd vertical mode and Q_{Tm0} the amplitude of the mode coordinate associated with the 2nd torsional mode. Considering again (18), ψ_m is the relative phase between the two mode coordinates.

To determine the oscillation amplitudes of the two mode coordinates in (18) both the values are multiplied by an amplification factor α. As aforementioned, amplitudes of limit cycles are associated with the equilibrium between energies introduced and removed from the system. Therefore, α can be identified by minimizing the difference between the energy introduced by the aerodynamic forces and the energy adsorbed with internal damping in one oscillation cycle. Being T_m the time period of the oscillation obtained as $2\pi/\omega_m$, this means:

$$E = \int_{T_m} \dot{\mathbf{q}}^T \mathbf{Q_a}(\mathbf{q}, \dot{\mathbf{q}})dt + \int_{T_m} -\dot{\mathbf{q}}^T [\mathbf{R}]\dot{\mathbf{q}}dt = \min \tag{19}$$

In (19) the vector of mode coordinates $\mathbf{q}$ is obtained summing up the vector of the static solution $\mathbf{q_s}$ referred to the wind speed v_m and the vector $\bar{\mathbf{q}}$ whose components are null except for $\bar{q}_V$ and $\bar{q}_T$. Taking into account the static solution is extremely important: considering that the bundle presents two I-type suspensions at the extremity, changing mean wind speed has a significant impact on the static angle of attack of the bundle which in turn influence the level of energy introduced by aerodynamic forces.

Referring to (19), the effect of aerodynamic forces on the mode coordinates is expressed through the term $\mathbf{Q_a}$, defined in (9), while the structural damping matrix **[R]** has been defined in (11). Equation (19) is solved iteratively through a minimization algorithm; the initial guess for the parameter α should be large enough to avoid convergence to α=0 which is a trivial solution of the problem.

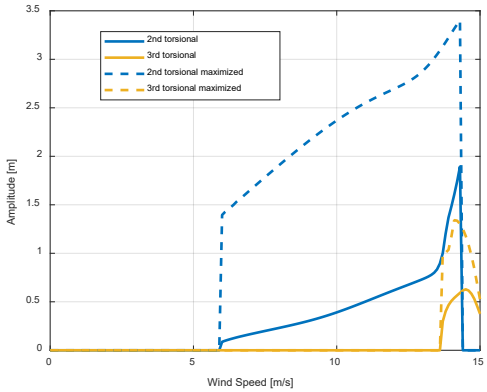

Fig. 11 Oscillation amplitudes predicted for 2nd and 3rd vertical-torsional unstable modes

Fig. 11 shows the amplitudes of oscillation predicted with the energy method. The blue continuous line (appearing for wind speeds slightly below 6 km/h) represents the maximum oscillation amplitude along the span associated with the 1st unstable mode; this mode is a combination of modes 3 and 4 of Table 4 (i.e. 2nd torsional and 2nd vertical) and maximum oscillation is recorded at ¼ the span length. The amplitude of oscillation displays an increasing trend with wind speed reaching a maximum of 1.9 m at 14.3 m/s. The orange continuous line refers to the 2nd unstable mode, appearing for wind speeds above 13 m/s; in this case the maximum oscillation is recorded at the span center as the unstable mode is a

combination of modes 6 and 7 of Table 4 (i.e. 3rd torsional and 3rd vertical); the predicted amplitude of oscillation presents a local maximum of 0.63 m at 14.5 m/s. It should be reminded that oscillation amplitudes are determined considering one unstable mode at a time.

As the predicted amplitudes are not so small, it is reasonable to assume that the modes resulting from a linear analysis and might be not fully suitable for describing the dynamics of the bundle during the limit cycle. The relative phases and amplitudes between mode coordinates in the limit cycle could change due to non-linearities introduced by large displacements. Therefore it could be useful to explore the effect of different mode shapes by changing amplitudes or relative phase in equation (18). In particular, following a conservative approach, it could be interesting to estimate the oscillation amplitudes when the torsional and the vertical displacement combine in the worst possible way. Considering the mechanism of energy introduction associated with flutter instability, this means introducing a relative phase of $-\pi/2$ in equation (18) in place of ψ_m. The result of the procedure leads to the dotted lines of Fig. 11. The energy method shows that, with the proper relative phase between torsional and vertical mode shape, maximum oscillations for the 1st unstable mode would reach 3.4 m. As far as the 2nd unstable mode is concerned, the same procedure leads to maximum oscillations in the order of 1.3 m. The differences between the continuous and dotted lines in Fig. 11, indicate that the relative phase between vertical and torsional displacement obtained with the linear analysis is quite far from the critical one in particular for the 1st unstable mode.

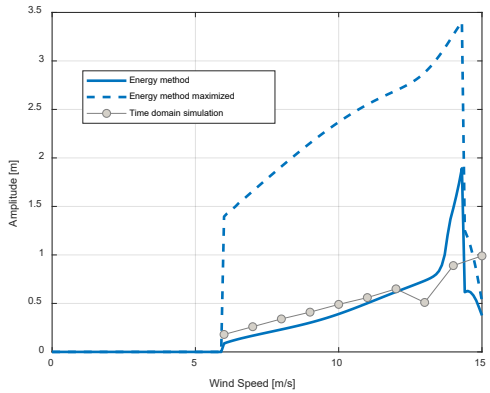

Fig. 12 comparison between oscillations amplitudes predicted through energy method and time domain simulations.

Fig. 12 reports a comparison between the oscillation amplitudes predicted with energy method and time-domain simulations. As in Fig. 11, the continuous line refers to the modes derived directly from the linear analysis while the dotted line refers to the modes modified to maximize energy introduction. It can be noticed how, when relying on direct output of linear analysis, the energy method provides reasonable estimates for the oscillation amplitudes, especially for wind speeds up to 14 m/s. There are then over estimations and underestimations between 14 m/s and 15 m/s. Results can be considered satisfying, especially when the 1st unstable mode is involved: relative phase between vertical and torsional modes obtained in time-domain simulations are quite similar to those resulting from the linear analysis. The oscillation amplitudes for the 2nd unstable mode are better estimated when the $\pi/2$ relative phase is assumed in the energy method.

VI. Conclusions

The paper described a modal model of the interaction between a 4-conductor bundle and turbulent wind, able to reproduce the phenomenon of galloping associated with ice formation. The model is based on a finite-element scheme used to extract the mode parameters of the entire bundle; the eigenmodes of the bundle are then processed to obtain the mode shapes of an equivalent super-conductor. The motion of this last is described through its first 8 mode coordinates.

Wind tunnel tests were carried out to determine how ice formation affects the aerodynamic coefficients of the conductor bundle. These data were introduced in the modal model allowing to reproduce the onset of galloping instability associated with combination of torsional and vertical displacements. In addition the experimental tests were used for model validation.

The model was then used to analyze a case study, aiming at predicting the onset speed of galloping instability and the maximum oscillation amplitudes of a four-conductor bundle with given boundary conditions. Two methods were adopted to obtain this goal: the first one is based on time-domain simulations, the second one on an energy approach. This last estimates oscillation amplitudes on the basis of the equilibrium between energy introduced in one cycle by aerodynamic forces and the energy dissipated by internal damping. The energy approach hypothesizes that the relative amplitudes and phases between vertical and torsional mode coordinates in a limit cycle can be derived from the eigenvector determined through a modal analysis.

Comparisons between the results of time-domain simulations and energy method revealed how the energy method could be used to obtain a reasonable estimates of bundle oscillations and how the same method can be regarded as a useful tool to speed up the settings definition (position, mass, length) of controlling devices such as detuning pendulums.

VII. References

[1] D. G. Havard, J. C. Pohlman, Five Year'field trials of detuning pendulums for galloping control, IEEE Transaction on Power Appartus and Systems, Vol. PAS-103, No 2, pp 318-327, 1984

[2] J. L. Lilien, H. Dubois, F. Dal Maso, General mathematical formulation for overhead line galloping, AI; study day on galloping, 1989

[3] C.B. Rawlins, Numerical studies of the galloping stability of single conductors, Technical paper n30 Alcoa Conductor Products Company, Spartanburg, SC, 1993

[4] A. Leblond, B. Lamarche, D. Bouchard, B. Panaroni., M. Hamel, Development of a Portable De-Icing device for overhead ground wires". "Proceedings of the Seventh International Workshop on Atmospheric Icing of Structures. Montreal 2005.

[5] EPRI Transmission Line Reference Book – Wind-Induced Conductor Motion, Second Edition, Chapter 4: Galloping Conductors, 2009

[6] , J. P. Den Hartog Transmission line vibration due to sleet. Trans. AIEE, 51:1074–1086, 1932

[7] J. C. R. Hunt, D. J. W. Richard, Overhead Line oscillations and the effect of aerodynamic dampers IEEE Trans on PAS, Vol 116, No 11 pp 1869-74, 1969

[8] J. C. R. Hunt, M. Rowbottom, Meteorological Conditions associates with the full span galloping oscillations of overhead transmission lines. Proceedings IEE, Vol 120, No 8, pp. 874-6, 1974
[9] D.G. Havard, C.J. Pon, Use of detuning pendulums for control of galloping of single conductor and two and four conductor bundle lines. Fifth International Workshop on Atmospheric Icing of Structures, Tokyo 1990
[10] G. Diana, F. Cheli, A. Manenti, F. Resta, M. Bocciolone, 1999, "The aeroelastic behavior of the OHTL expanded bundle", 3rd Int. Symp. on Cable Dynamics, Trondheim, 1999.
[11] M. Belloli, S. Melzi, S. Negrini, G. Squicciarini, "Numerical Analysis of the Dynamic Response of a 5-Conductor Expanded Bundle Subjected to Turbulent Wind", IEEE Transactions on Power Delivery, vol. 25, p. 3105-3112, ISSN: 0885-8977, doi: 10.1109/TPWRD.2010.2056396
[12] J. J. Moré, B. S. Garbow, and K. E. Hillstrom, User Guide for MINPACK 1, Argonne National Laboratory, Rept. ANL-80-74, 1980.

VIII. BIOGRAPHIES

Giorgio Diana: SM, born 1936, Mechanical Eng. Degree 1961, Professor of Applied Mechanics since 1971. Giorgio Diana received his Degree in Mechanical Engineering from Politecnico di Milano in 1961. Since 1971 he is has been a full professor of Applied Mechanics. In December 2010 he has been appointed Professor Emeritus of Politecnico di Milano.
At present he is member of the Scientific Committee of the Politecnico di Milano Wind Tunnel. Since 2010 he teaches the course of Wind Engineering. Member of IEEE, IABSE, and Cigre (Chairman of WG B2-58). His actual main research fields are: bridges dynamics, railway vehicle - infrastructure dynamic interaction and aeroelasticity problems. The results of the research and activities in these fields are reported in about 300 papers published on International Reviews as well as Keynote Lectures held at several International Conferences.
Prof.. Diana received several international awards, among which : the 2009 Robert H. Scanlan Medal from the American Society of Civil Engineers (ASCE) and the 2014 IAWE Senior Award with Davenport medal, from IAWE – The International Association of Wind Engineers.

Alessandra Manenti: born 1958, Mechanical Eng. Degree 1982, PhD. in Applied Mechanics 1987, Researcher, then Professor, in Mech. Measurements since 1986. Since 2002 she is with the School of Industrial and Information Engineering of Politecnico di Milano. In 2012 she left the Mechanical Measurements Scientific Group and joined the Applied Mechanics Scientific Group. Her research works are in the field of experimental and analytical behavior of overhead transmission line conductors, rotor-dynamics, statistical data analysis. She authored more than 80 scientific papers published on national or international reviews and presented to international conferences. She is a member of various Cigré B2 Working Groups. She is a member of the Italcertifer (Consortium among Trenitalia (FS Group), RFI (FS Group) and some Universities for the certification in the Rolling Stock field) Administration Board. She is the responsible at the Department of Mechanics of Politecnico di Milano for the laboratory tests of conductors and fittings.

Stefano Melzi: M '09, received M.Sc degree in Mechanical Engineering in 1999 and Ph.D. degree in Applied Mechanics in 2003 from Politecnicco di Milano. He became Assistant Professor in 2001 and he is Associate Professor since 2014. Since His research activity deals in general with dynamics of mechanical systems and, in particular, on the dynamics of ground vehicles and interaction of wind with overhead transmission lines. He is author of almost 150 publications almost entirely at international level.